Appl Phys B (2010) 100: 833–839
DOI 10.1007/s00340-010-4172-x

Applied Physics B
Lasers and Optics

Analysis of tunable bandgaps in liquid crystal-infiltrated 2D silicon photonic crystals

J. Cos · J. Ferré-Borrull · J. Pallarès · L.F. Marsal

Received: 11 December 2009 / Revised version: 7 July 2010 / Published online: 19 August 2010

Abstract We present a theoretical study on two-dimensional photonic crystals composed of silicon and the E7 liquid crystal. We analyze how the optical axis orientation of the liquid crystal influences the photonic bands and bandgaps, for the case when the Maxwell equations can be decoupled into the TE and TM modes. We consider two different structures, a triangular lattice of E7 liquid crystal cylinders in a silicon background and a triangular lattice of silicon cylinders in an E7 liquid crystal background. The effect of the liquid crystal anisotropy on the geometry of the irreducible Brillouin zone allows us to propose a simplified way to calculate the photonic bandgaps. Results show that the bandgap width and center frequency have a 60° periodicity for both structures. Using the plane-wave expansion method, we determined the maximum bandgap and the optimal radius of the cylinders for each structure. Finally, for the second structure, we propose an optical switch with a 50% duty cycle. These structures can be applied to design tunable photonic devices.

1 Introduction

Photonic crystals (PCs) are periodic dielectric or metal-dielectric synthetic structures designed to control the propagation of electromagnetic waves in the same way as the periodic potential in semiconductor crystals affects the electron motion by defining allowed and forbidden energy bands. Since first proposed [1, 2] considerable advances have been achieved in tailoring material architectures toward a versatile structural control of light propagation. Such structures have been long studied and widely applied as semiconductor lasers and solar cells [3], high-quality resonator and filters [4], optical fibers [5], etc. For most applications, photonic crystals with tunable or switchable optical properties are desired.

Several structures combining photonic crystals with nonlinear optical (NLO) materials or liquid crystals (LC) materials have been proposed [6–8]. In the former case, a high-intensity control signal with frequency outside the bandgap changes the properties of the crystal [9]. Among available strategies, liquid crystals (LC) are recognized as unique materials that combine birefringence and periodic spatial ordering with a pronounced sensitivity to external fields [10].

Besides the tuning properties of the liquid crystals, the optical anisotropy is another fundamental property than can be taken as a degree of freedom in the design of applications. In the last years there are several works that exploit this anisotropy in the theoretical [11–13] or experimental [14–18] analysis of photonic crystals. However, only a few studies on LC infiltrated 2D photonic structures are devoted to study the gap maps and tunable capabilities as a function of the geometrical parameters of the photonic crystal for direct and inverse structures.

The aim of the present paper is to study and analyze the viability of tunable devices based on liquid crystal and silicon. To this end, we study the gap maps as a function of the geometrical parameters of the photonic crystal (radius of the scatterers), the optical axis angle of LC and the PC configuration (holes infiltrated with liquid crystal or rods surrounded by liquid crystal). The knowledge of these properties is important since they have to be taken into account when designing tunable devices based on liquid crystal-

J. Cos · J. Ferré-Borrull · J. Pallarès · L.F. Marsal (✉)
Nanoelectronic and Photonic Systems, Department of Electronic, Electric and Automatic Control Engineering, Universitat Rovira i Virgili, Avda. Països Catalans 26, 43007 Tarragona, Spain
e-mail: lluis.marsal@urv.cat
Fax: +34-977-559605

infiltrated photonic crystals. One of the most important aspects in this study is that the optical anisotropy of the liquid crystal component induces a change in the symmetry properties of the photonic crystal lattice. For this reason, Sect. 2 is devoted to introduce the mathematical basis of our models and to define a computationally efficient method to calculate the photonic bandgaps in structures with anisotropic component. Then, in Sect. 3 the photonic bandgap properties are studied. From the analysis of the gap maps conclusions on the tolerance in the photonic crystal geometric parameters, or proposals for new devices can be extracted.

2 Theoretical background

2.1 Numerical method

Let us consider a 2D photonic crystal with periodicity in the x–y plane and uniform refractive index variation in the z direction. The 2D photonic crystals we study in this work are composed of an isotropic component (Silicon) and an uniaxial anisotropic component (E7 liquid crystal). The photonic crystal structure we have chosen is the triangular lattice, since it has larger photonic bandgap (PBG) for the TE modes than other geometries as square, honeycomb or Kagome [19].

We want to study structures where the TE and TM polarizations can be decoupled. We have considered TE and TM polarizations with respect to the x–y plane. In these cases TE components are E_x, E_y and H_z while TM components are H_x, H_y and E_z [20]. For the decoupling, it is important to have the anisotropic materials in such orientation that the polarizations can be decoupled and that the direction of the extraordinary axes influences the photonic bands. Following [21], Maxwell's equations can only be decoupled in two cases: (i) when the optical axis is oriented along the rods of the 2D photonic crystal, and (ii) when the optical axis is perpendicular to the rods. Furthermore, only in the second case, the direction of the optical axis influences the photonic band structure. In this second case, the dielectric tensor can be decomposed into two parts, one for the x–y plane, (ε_r) and one for the z direction (ε_z).

$$\varepsilon_z(\mathbf{r}) = \varepsilon_{33}(\mathbf{r}) = \varepsilon_o$$

$$\varepsilon_r(\mathbf{r}) = \begin{pmatrix} \varepsilon_{11}(\mathbf{r}) & \varepsilon_{12}(\mathbf{r}) \\ \varepsilon_{21}(\mathbf{r}) & \varepsilon_{22}(\mathbf{r}) \end{pmatrix} = \begin{pmatrix} \varepsilon_o \sin^2\alpha + \varepsilon_e \cos^2\alpha & (\varepsilon_o - \varepsilon_e)\cdot\cos\alpha\cdot\sin\alpha \\ (\varepsilon_o - \varepsilon_e)\cdot\cos\alpha\cdot\sin\alpha & \varepsilon_o \cos^2\alpha + \varepsilon_e \sin^2\alpha, \end{pmatrix} \tag{1}$$

where α is the angle between the optical axis and the x-axis as it is stated in Fig. 1. Applying the planar wave expansion

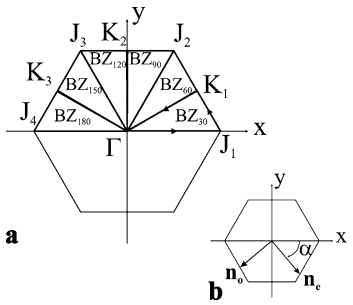

Fig. 1 (**a**) Definition of the BZ sets for the accurate and efficient calculation of the photonic bandgaps of the studied photonic crystals. (**b**) (*Inset*) Definition of the angle α that characterizes the LC optical axis orientation

(PWE) method to the Maxwell equations, the eigenequations for TE and TM polarizations, respectively, are obtained:

$$\sum_{\mathbf{G}'} (\mathbf{k}+\mathbf{G}) \bullet \varepsilon^{-1}_{r\mathbf{G}\mathbf{G}'} (\mathbf{G}-\mathbf{G}') \bullet (\mathbf{k}+\mathbf{G}') \cdot H_{z,\mathbf{k}}(\mathbf{G}') = (\omega/c)^2 \cdot H_{z,\mathbf{k}}(\mathbf{G}) \tag{2a}$$

$$\sum_{\mathbf{G}'} \varepsilon^{-1}_{z\mathbf{G}\mathbf{G}'} (\mathbf{G}-\mathbf{G}') \cdot |\mathbf{k}+\mathbf{G}| \cdot |\mathbf{k}+\mathbf{G}'| \cdot F_{z,\mathbf{k}}(\mathbf{G}') = (\omega/c)^2 \cdot F_{z,\mathbf{k}}(\mathbf{G}) \tag{2b}$$

where the $H_{z,\mathbf{k}}$ are the expansion coefficients for the magnetic field in the TE polarization and equivalently for the $F_{z,\mathbf{k}}$, the electric field and the TM polarization. The ω is the angular frequency. The $\varepsilon^{-1}_{z\mathbf{G}\mathbf{G}'}$ and $\varepsilon^{-1}_{r\mathbf{G}\mathbf{G}'}$ are, respectively, the Fourier Transform of the inverse of $\varepsilon_{33}(\mathbf{r})$ and $\varepsilon_r(\mathbf{r})$ and c is the speed of light in vacuum. These Fourier components are defined for two-component systems as:

$$\varepsilon^{-1}(G) = \begin{cases} (f\cdot\varepsilon_c^{-1} + (1-f)\cdot\varepsilon_b^{-1}) & \text{for } G = 0 \\ (\varepsilon_c^{-1} - \varepsilon_b^{-1})\cdot S(G) & \text{for } G \neq 0 \end{cases}, \tag{3}$$

where ε_c is the element of the dielectric tensor corresponding to the material of the cylinders, ε_b is the same dielectric tensor element corresponding to the background material, f is the filling factor and $S(G)$ is the Fourier transform of the unit cell. It important to note that $S(G)$ relies only on the geometry of the cylinders and on the lattice structure. Since we analyzed a triangular lattice with circular rods, Table 1 shows the geometrical properties such lattice [22], where a and R are the lattice constant and the rod radius respectively.

It is worth explaining in detail how to obtain the ε^{-1}. Thus, for instance, to obtain $\varepsilon^{-1}_{z\mathbf{G}\mathbf{G}'}$ for a 2D photonic crystal consisting of an isotropic background with holes filled with liquid crystal, and where the liquid crystal optical axis is in the x–y plane, ε_c is ε_o and ε_b is the background dielectric constant. Instead, for $\varepsilon^{-1}_{r\mathbf{G}\mathbf{G}'}$ four elements must be calculated. Thus, in the isotropic background-anisotropic cylin-

Table 1 Geometrical properties of a triangular lattice photonic crystal with cylindrical scatterers

Base vector	$\mathbf{a}_1$	$a\hat{\mathbf{x}}$
	$\mathbf{a}_2$	$a(\frac{1}{2}\hat{\mathbf{x}} + \frac{\sqrt{3}}{2}\hat{\mathbf{y}})$
Reciprocal lattice base vector	$\mathbf{b}_1$	$(2\pi/a)(\hat{\mathbf{x}} - \frac{1}{\sqrt{3}}\hat{\mathbf{y}})$
	$\mathbf{b}_2$	$(2\pi/a)\frac{2}{\sqrt{3}}\hat{\mathbf{y}}$
Filling factor f		$\frac{2\pi}{\sqrt{3}}(R/a)^2$
$S(G)$		$2f\frac{J_1(GR)}{(GR)}$

ders configuration mentioned above, to obtain the x–x element of $\varepsilon^{-1}_{r\mathbf{GG}'}$ (3) must be applied with $\varepsilon_c = \varepsilon_{11}(\boldsymbol{r})$ and ε_b the background dielectric constant, while to obtain the x–y element $\varepsilon_c = \varepsilon_{12}(\boldsymbol{r})$ and $\varepsilon_b = 0$ must be considered.

From (2) and (3) it can be seen that the z component of the dielectric tensor appears only in the eigenequation for TM polarization, while the x–y component appears only in the eigenequation for TE polarization. Furthermore, only the eigenequation for the TE polarization is affected by the orientation of the optical axis.

2.2 Brillouin zone and geometry

Due to the anisotropy of the liquid crystal and its influence on the TE polarization, the Irreducible Brillouin Zone (IBZ) usually considered for isotropic 2D photonic crystals with triangular lattice it is not sufficient to represent the whole First Brillouin Zone (FBZ). In fact, in Ref. [21] it is demonstrated that the IBZ depends on the LC optical axis orientation. This work provides with a means for calculating the photonic bandgaps based in choosing the IBZ depending on the LC optical axis orientation and calculating all the **k** points within the IBZ.

In this work we propose an alternative method to calculate the photonic bandgaps based on calculating the bands along the **k** in the main high symmetry directions of the First Brillouin Zone. With this aim we have divided the upper half of the FBZ in sets of **k** points denominated BZ_{30}, BZ_{60}, BZ_{90}, BZ_{120}, BZ_{150}, and BZ_{180}, as it is shown in Fig. 1a. The set BZ_{30} consists of the **k** points along the path Γ-J_1-K_1-Γ, the set BZ_{60} to the path Γ-K_1-J_2-Γ, and analogously for the other sets. Only the upper half is meaningful, since for all orientations of the optical axis the system retains the 180° rotation symmetry. Taking into account that the symmetry of the photonic crystal is reduced by the fact that the liquid crystal sets a preferential direction on the structure, the maximum and minimum frequencies of the photonic bands will appear at the points along the paths included in the BZ sets. This permits to obtain the photonic bandgap without calculating the photonic bands for all **k** points of the FBZ, resulting in a less time-consuming numerical method. Thus, the photonic bandgap limits and its width are determined by taking the maximum frequency for the lower band and the minimum frequency of the upper band, at the calculated points.

3 Theoretical analysis of the bandgaps of photonic crystals infiltrated with LC

Using this method we have analyzed the photonic bang gap properties of a photonic crystal composed of silicon ($n_{Si} = 3.478$ at 0.8 eV) with a triangular lattice of circular holes with radius R and lattice constant a, infiltrated by E7 Liquid Crystal ($n_o = 1.522$, $n_e = 1.706$). Typical fabricated silicon photonic crystals lattice dimensions are on the order of few microns [18], with hole diameters of some hundreds of nanometers. On the other hand, the E7 molecule length is about 2–3 nm, which ensures the mobility of the LC within the hole and thus its control by means of external electric fields.

We have carried the analysis of the gap maps as a function of the hole radius a and of the LC director angle α. The gap maps were calculated for α between 0° and 60°. We use 529 plane-waves in order to guarantee convergence for the 8 first bands within an error smaller than 1%. Due to the low contrast index between silicon and liquid crystal there exists only one photonic bandgap between the 1st and 2nd modes.

Figure 2a shows the gap maps for TE polarization for $\alpha = 0°$ and $\alpha = 30°$, which correspond to the biggest difference between the gap maps. The solid line delimits the area corresponding to the gap map for $\alpha = 0°$, while the dashed line corresponds to the gap map for $\alpha = 30°$. The gap map for any other angle is included within the gap map for $\alpha = 0°$ and includes the gap map for $\alpha = 30°$. The arrows indicate the radius corresponding to the maximum bandgap width for the two angles i.e. for $\alpha = 0°$ maximum bandgap ($\Delta\omega a/2\pi c = 0.0581$) is obtained at $R/a = 0.401$ and for $\alpha = 30°$ maximum bandgap ($\Delta\omega a/2\pi c = 0.0521$) is obtained at $R/a = 0.395$. Figure 2b shows a detail of the graph in Fig. 2a, for the range of R/a where the bandgap is maximum. As it can be seen, the change of the gap width with the LC optical axis orientation is small, and it is mainly caused by the decrease of the upper edge of the bandgap with increasing α. In this figure the difference between the radii at which the gap is maximum can be observed. Finally, Fig. 2c shows a detail of the gap maps in the range of R/a around the value where the gap closes. As it can be seen, the gap closes at different R/a for different LC optical axis orientations.

The dependence of the band gap limits with the LC orientation angle can be explained by the analysis of the H_z component field distribution for the photonic bands corresponding to such limits. As we commented before, the gap

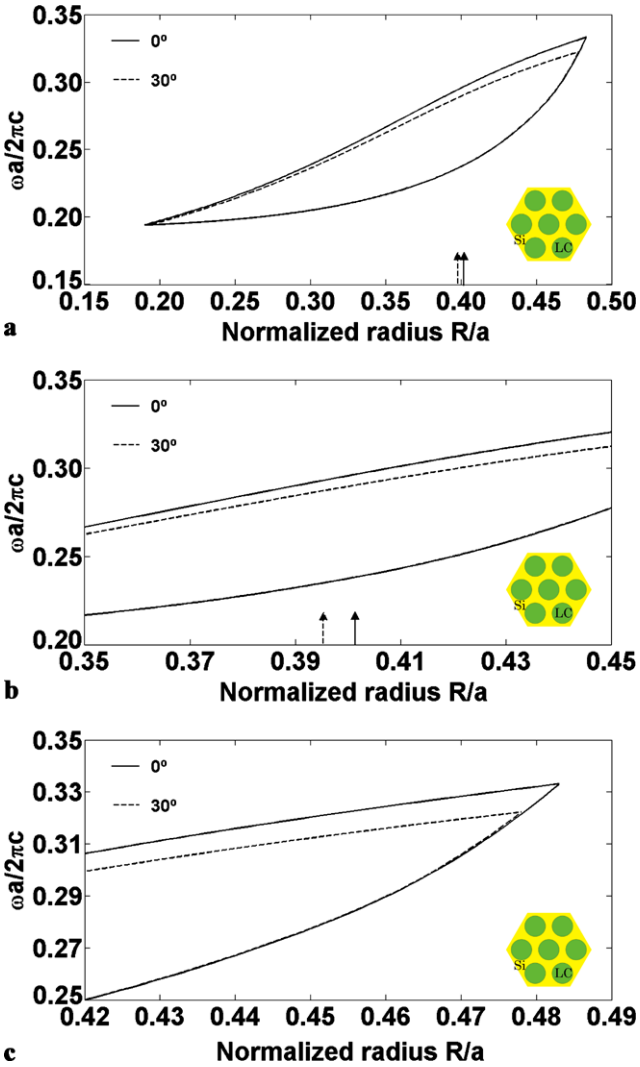

Fig. 2 (**a**) Photonic bandgap map for the TE polarization for $\alpha = 0°$ (*solid line*) and $\alpha = 30°$ (*dashed line*). The arrows indicate the R/a corresponding to the maximum gap width. (**b**) Detail of the region around the maximum gap width. (**c**) Detail of the region of R/a with the biggest difference between the gap maps at $\alpha = 0°$ and $\alpha = 30°$. Insets show a schematic view of the structure

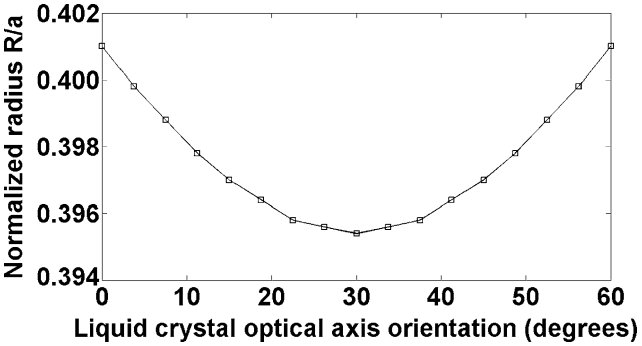

Fig. 3 Radius corresponding to the maximum bandgap as a function of the LC optical axis orientation, α

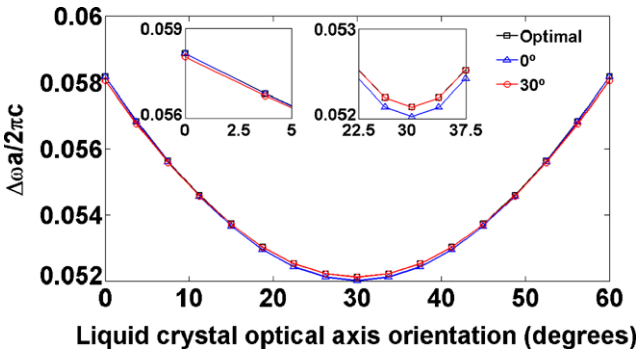

Fig. 4 Bandgap width between 1st and 2nd TE modes versus LC optical axis orientation for (i) the radius corresponding to the maximum bandgap at each α (*black square marker*), (ii) the radius giving the maximum width at $\alpha = 0°$ (*blue triangular marker*) and (iii) the radius giving the maximum width at $\alpha = 30°$ (*red circular marker*). The *insets* show a detail of the ranges of α where the difference between the three curves is maximum

limits are formed by the first and second photonic bands (see supplementary material).

The field distribution for the first band shows a strong confinement in the circular holes, with almost circular symmetry for $\alpha = 0°$. When α changes the field distribution for the first band does not change appreciably. The almost circular symmetry of the first band field distribution causes it to be insensitive to the LC optical axis orientation, and thus the lower band gap limit is constant.

The field distribution for the second band shows a node along one diameter of the circular holes, while the Si shows a high field amplitude for $\alpha = 0°$. When α changes the field distribution for the second band is slightly dependent on α, but the field is mainly confined in the Si, thus, even though a corresponding change in upper band gap limit frequency is observed, it is nevertheless small.

Figure 3 shows the radius corresponding to the maximum bandgap as a function of the LC optical axis orientation, α. As it can be seen, the influence of α is very small: the maximum relative difference between the radius observed in Fig. 3 is only 1.4%. This means that a tunable device based on this structure designed to have the maximum bandgap should have a radius in the range shown in Fig. 3. However, an actual device must have a fixed radius, and therefore the bandgap of the device will change with the LC optical axis orientation. In Fig. 4, the influence of having a fixed radius on the bandgap width is depicted. The graph shows the bandgap width as a function of α. The three curves correspond to: (i) the bandgap obtained with the optimal radius at the given LC optical axis orientation (squares), (ii) the bandgap obtained for the fixed radius giving the maximum width for $\alpha = 0°$, $R/a = 0.401$ (triangles) and (iii) the bandgap obtained for the fixed radius giving the maximum width for $\alpha = 30°$, $R/a = 0.395$ (circles). As it can be seen, the bandgap width has a very similar behavior in the three

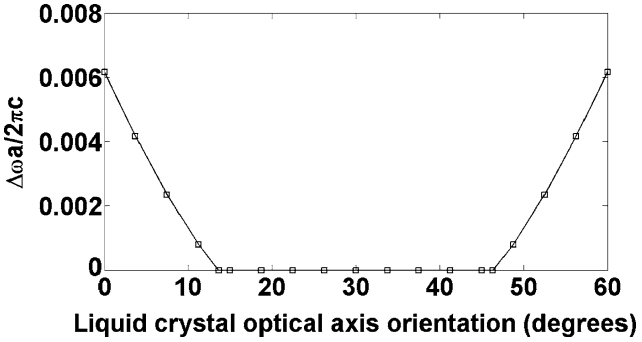

Fig. 5 Bandgap width as a function of the LC optical axis orientation for $R/a = 0.48$

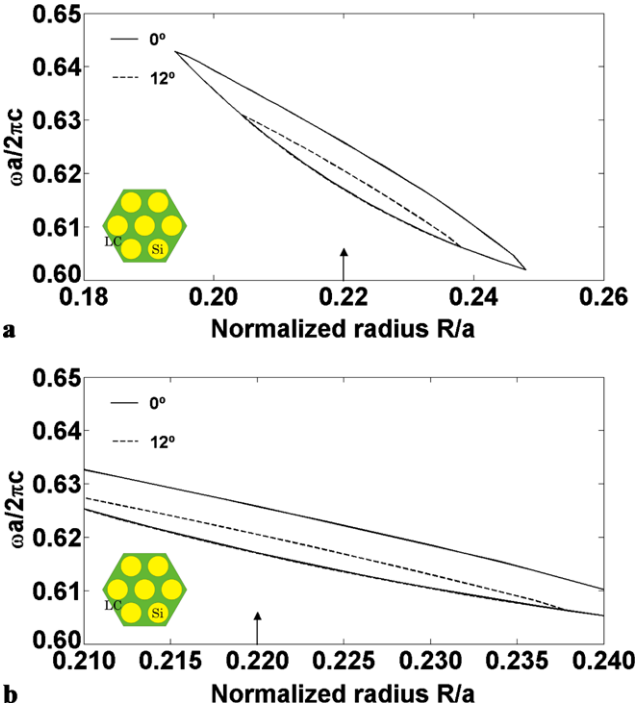

Fig. 6 (**a**) Photonic bandgap map for the TE polarization for $\alpha = 0°$ (*solid line*) and $\alpha = 12°$ (*dashed line*). The *arrow* indicates the R/a corresponding to the maximum gap width for all α. (**b**) Detail of the region around the maximum gap width. *Insets* show a schematic view of the structure

cases. As it can be seen in the insets, the maximum difference between the bandgap width for a fixed radius and the optimal width is 0.2%. This means that there is a tolerance in the size of the radius of the holes in the photonic crystal structure: the bandgap width dependence with the LC optical axis orientation will be almost invariant as long as the radius lies within the range of optimal radii in Fig. 3. Figure 4 also shows that, for this range of radius, the bandgap width changes a maximum of an 11.6% with the LC optical axis orientation.

Another interesting feature of this structure is the fact that the gap can be opened and closed with the LC optical axis orientation. In Fig. 2c it has been shown that there is a range where, for a given R/a, the gap closes at some angle between $\alpha = 0°$ and $\alpha = 30°$. By choosing appropriately the radius of the cylinder a photonic crystal can be designed such that its bandgap can be closed or opened up to a certain width, as a function of the LC optical axis orientation. Figure 5 shows the gap width as a function of the LC optical axis orientation for $R/a = 0.48$. For this radius the gap is closed for α between 24° and 36° and reaches a maximum gap width of $\Delta\omega a/2\pi c = 0.0062$ for $\alpha = 0°$ and $\alpha = 60°$. Changing the scatterer radius results in a change of the maximum gap width and of the range of α where the gap closes.

The previous result suggests a structure with a tunable bandgap that can be open and closed. However, it has a remarkable drawback: the tolerance in the value of the radius is very small. This can be explained by observing Fig. 2c: an increase of 1% in the R/a results in a structure without any bandgap, or a decrease in 1% in R/a results in a structure where the gap never closes. This makes the actual fabrication of a device based on this feature very difficult.

In the following, we study an alternative structure that shows a better fabrication tolerance: a photonic crystal composed of a triangular array of silicon cylinders surrounded by E7 liquid crystal. As in the previous case, the liquid crystal optical axis is maintained in the x–y plane and the structure is tuned by varying the LC optical axis angle with the y-axis, α. Figure 6a shows the gap maps for $\alpha = 0°$ and $\alpha = 12°$. The results show that, as the angle α increases, the gap map is reduced until the gap closes for all radius values between $\alpha = 24°$ and $\alpha = 30°$. This behavior is symmetric with respect the angle $\alpha = 30°$ and repeats every 60°. The arrow indicates the R/a corresponding to the maximum width for all α. Figure 6b shows a detail of the range of R/a where the gap is maximum.

This dependence of the gap with the optical axis orientation of the LC suggests that it can be applied as a switch. In this case, the radius of the silicon cylinders can be chosen to modulate the duty cycle of the switch, this is: the range of angles where the gap is closed. Choosing the radius also defines the maximum value of the achievable bandgap width and for $R/a = 0.220$ this achievable width is maximum ($\Delta\omega a/2\pi c = 0.0087$). Figure 7 shows the bandgap width for such radius of the silicon cylinders (squares) as a function of the angle α. For this radius, the corresponding duty cycle is 80% opened/20% closed. If a 50% duty cycle is desired, the radius should be $R/a = 0.206$. The corresponding bandgap width can be seen in Fig. 7 as well.

Analogue to the previous structure, the dependence of the band gap limits with the LC orientation angle can be again explained by the analysis of the H_z component field distribution of the photonic bands corresponding to such limits. In this case, the gap limits are between the fourth and fifth photonic bands (supplementary material).

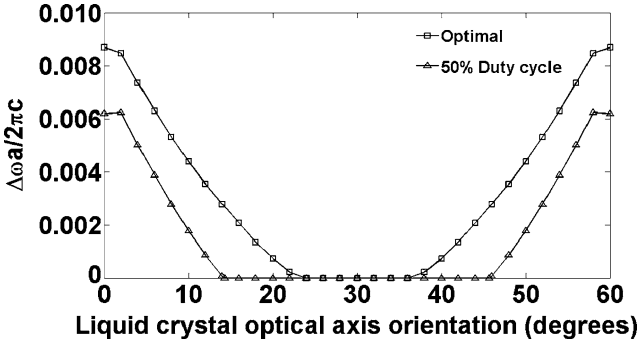

Fig. 7 Bandgap width between 4th and 5th TE modes versus LC optical axis orientation for (i) the radius corresponding to the maximum bandgap for all α (*square marker*), (ii) the radius giving a 50% duty cycle (*triangular marker*)

The field distribution for the fourth band for $\alpha = 0°$ shows a strong confinement in the Si, with circular symmetry and an appreciably low amplitude in the LC. The field distribution for the fourth band for $\alpha = 30°$ does not change appreciably. The low band gap limit has not dependence with the LC orientation due to the low field amplitude for the fourth band in the LC (supplementary material).

The fifth band for $\alpha = 0°$ shows a dipole shape along a diameter of the Si cylinders in the Γ-M direction while the LC region shows field maxima and minima. For $\alpha = 30°$ the field distribution for the fifth band shows a nodal line in the Γ-K direction (supplementary material). The remarkable change in the field distribution for the fifth band gives rise to the higher tunability observed for this structure.

4 Conclusions

We have studied the photonic bandgap tunability properties of 2D photonic crystal structures based on silicon and liquid crystal components. The orientation of the liquid crystal is such that the optical axis lies in the plane of periodicity of the photonic crystal. In this configuration the Maxwell equations can be decoupled in TE and TM modes and the optical axis orientation only influences the TE bands. We have studied two different structures: (i) a triangular lattice of E7 liquid crystal cylinders in a silicon background and (ii) the inverse structure i.e. triangular array of silicon cylindrical rods in a E7 liquid crystal background.

The anisotropy of the liquid crystal causes that the Irreducible Brillouin Zone is different depending on the liquid crystal optical axis orientation. In order to obtain an accurate value for the bandgap limits, it has been necessary to define a method to calculate the bandgaps of the structures based on the plane-wave expansion and on the calculation of the bands along paths of high symmetry in the First Brillouin Zone.

For the first structure, the TE bandgap appears between the 1st and 2nd bands and it has a 60° periodicity with the LC optical axis orientation, α. Results show that variation of the obtained bandgap is very small (1.4%) and largest bandgap ($\Delta\omega a/2\pi c = 0.0581$) is obtained for $\alpha = 0°$. For angles increasing up to $\alpha = 30°$ the bandgap width decreases because of the decrease of the upper limit. However, from $\alpha = 30°$ to $\alpha = 60°$ there is a symmetrical behavior and the bandgap increases when increases α. Results also shown that the maximum bandgap depends very slightly on the radius of the LC cylinders. This demonstrates that, using any radius in the range of optimal radii, the variation of the bandgap width presents an undistinguishable dependence with α.

In contrast, the second structure i.e. silicon rods surrounded with LC presents a bandgap that is opened between $\alpha = 0°$ and $\alpha = 24°$ and it is closed between $\alpha = 24°$ and $\alpha = 30°$. For $R/a = 0.220$, we obtain the maximum bandgap ($\Delta\omega a/2\pi c = 0.0087$). Otherwise this behavior can be used to design the desired duty cycle by adjusting the radius of cylinder appropriately, at the cost of having a narrower maximum bandgap.

The dependence of the band gap limits with the LC orientation angle has been explained by the analysis of the field distribution of the photonic bands corresponding to such limits. The results show that the change in the band gap limits depends not only on the field confinement in the LC but also on the field distribution symmetry.

Acknowledgements This work was supported by Spanish Ministry of Ciencia e Innovacion (MICINN) under grant number TEC2009-09551, HOPE CSD2007-00007 (Consolider-Ingenio 2010) and AECID-A/024560/09.

References

1. S. John, Phys. Rev. Lett. **58**, 2486 (1987)
2. E. Yablonovitch, Phys. Rev. Lett. **58**, 2059 (1987)
3. O. Painter, R.K. Lee, A. Scherer, A. Yariv, J.D. O'Brien, P.D. Dapkus, I. Kim, Science **284**, 1819 (1999)
4. R.D. Meade, K.D. Brommer, A.M. Rappe, J.D. Joannopoulos, Phys. Rev. B **44**, 13772 (1991)
5. J.C. Knight, J. Broeng, T.A. Birks, P.St.J. Russell, Science **282**, 1476 (1998)
6. K. Busch, S. John, Phys. Rev. Lett. **83**, 967 (1999)
7. H. Takeda, K. Yoshino, J. Appl. Phys. **92**, 5658 (2002)
8. I.S. Maksymov, L.F. Marsal, J. Pallarès, Opt. Quantum Electron. **38**, 149 (2006)
9. F. Cuesta-Soto, A. Martínez, J. García, F. Ramos, P. Sanchis, J. Blasco, J. Martí, Opt. Express **12**, 161 (2004)
10. S.M. Weiss, H.M. Ouyang, J.D. Zhang, P.M. Fauchet, Opt. Express **13**, 1090 (2005)
11. P. Kopperschmidt, Appl. Phys. B **73**, 717 (2001)
12. J. Arriaga, L. Dobrzynski, B. Djafari-Rouhani, R. Biswas, C.G. Ding, J. Appl. Phys. **104**, 063108 (2008)
13. J. Cos, J. Ferre-Borrull, J. Pallares, L.F. Marsal, Opt. Comm. **282**, 1220 (2009)
14. Ch. Schuller, J.P. Reithmaier, J. Zimmermann, M. Kamp, A. Forchel, S. Anand, Appl. Phys. Lett. **87**, 121105 (2005)

15. X. Sun, X. Tao, T. Ye, P. Sue, Y.-S. Szeto, Appl. Phys. B **87**, 267 (2007)
16. V.A. Tolmachev, T.S. Perova, S.A. Grudinkin, V.A. Melnikov, E.V. Astrova, Y.A. Zharova, Appl. Phys. Lett. **90**, 011908 (2007)
17. F. Genereux, S.W. Leonard, H.M. van Driel, A. Birner, U. Gösele, Phys. Rev. B **63**, 161101 (2001) (Rapid Communication)
18. S.W. Leonard, J.P. Mondia, H.M. van Driel, O. Toader, S. John, K. Busch, A. Birner, U. Gösele, V. Lehmann, Phys. Rev. B **61**, 2389 (2000) (Rapid Communication)
19. N. Susa, J. Appl. Phys. **91**, 3501 (2002)
20. J.D. Joannopoulos, S.G. Johnson, J.N. Winn, R.D. Meade, *Photonic Crystals: Molding the Flow of Light* (Princeton Univ. Press, Princeton, 2008)
21. G. Alagappan, X.W. Sun, P. Shum, M.B. Yu, D. den Engelsen, J. Opt. Soc. Am. A **23**, 2002 (2006)
22. P.G. Luan, Z. Ye, Condensed Matter **1**, 0105428 (2001)